Earthquakes and Structures, *Vol. 16, No. 2 (2019) 149-163*
DOI: https://doi.org/10.12989/eas.2019.16.2.149

High performance active tuned mass damper inerter for structures under the ground acceleration

Chunxiang Li* and Liyuan Cao

Department of Civil Engineering, Shanghai University, No. 99 Shangda Road, Shanghai 200444, P.R. China

(Received August 6, 2018, Revised December 24, 2018, Accepted December 27, 2018)

Abstract. By integrating an active tuned mass damper (ATMD) and an inerter, the ATMDI has been proposed to attenuate undesirable oscillations of structures under the ground acceleration. Employing the mode generalized system, the dynamic magnification factors (DMF) of the structure-ATMDI system are formulated. The criterion can then be defined as the minimization of maximum values of the DMF of the controlled structure for optimum searching. By resorting to the defined criterion and the particle swarm optimization (PSO), the effects of varying the crucial parameters on the performance of ATMDI have been scrutinized in order to probe into its superiority. Furthermore, the results of both ATMD and tuned mass dampers inerter (TMDI) are included into consideration for comparing. Results corroborate that the ATMDI outperforms both ATMD and TMDI in terms of the effectiveness and robustness. Especially, the ATMDI may greatly reduce the demand on both the mass ratio and inerter mass ratio, thus being capable of further miniaturizing both the ATMD and TMDI. Likewise the miniaturized ATMDI still keeps nearly the same stroke as the TMDI with a larger mass ratio. Hence, the ATMDI is deemed to be a high performance control device with the miniaturization and suitable for super-tall buildings.

Keywords: structural vibration control; active tuned mass damper inerter; high performance; particle swarm optimization; miniaturization; super-tall buildings

1. Introduction

Alleviating the dynamic response of civil engineering structures against earthquakes and winds has drawn the interest of many researchers in recent decades. Many passive, semi-active, active, and hybrid control devices have been developed. The core components of purely active control include a certain amount of external power or energy requirement and a decision-making process based on the sensed data on the actual vibration states of structures. For super-tall buildings, however, if the purely active control system is taken into account, then a large control force must be created and the power limitation of actuator prevents this system from being implemented. Among the passive devices available, the tuned mass damper (TMD) is one of the simplest and most reliable, typically consisting of an auxiliary mass (i.e., a SDOF mass block), a spring, and a viscous damper attached to the structure to be controlled. The TMD is a purely passive device by which the structural vibration energy is transferred to the TMD, without the need of any external power and with the low cost implementation. The resonance-based design criterion ensures that significant kinetic energy is transferred from the primary structure to the attached mass block and is eventually dissipated at the dashpot. To this end, the TMD tuning simultaneously involves a proper selection of the dashpot coefficient to ensure efficient energy dissipation, as a result, achieving the target of the structural dynamic response reduction. Basically, the TMD is tuned near the target resonance frequency of the mode generalized system in the specific vibration mode being controlled (referred here to as the structure, in practical terms, the SDOF structure), thus only damping one mode of the vibration. In the light of intensive researches and developments in recent years, the TMD has been recognized as one of the most widely used and accepted wind response control systems for super-tall buildings and bridges (Chung *et al*. 2013, Lu and Chen 2011a, 2011b, Casciati and Giuliano 2009). There is not a general agreement, instead, on the TMD effectiveness in reducing the earthquake-induced responses of structures. Effectively, under the narrow band excitations, such as winds and earthquakes with limited band frequency, the TMD is capable of enhancing performances of the protected structures; hence, when employing the TMD, the band of tuning frequency in which the structural vibration can be suppressed, or intitule the band of suppression frequency, is very narrow. This effectively also means that it is very important to accurately identify the natural frequency of the TMD or to provide tracking with an updating scheme because the control performance of the TMD depends extensively on how it is properly tuned to the natural frequency of a structure. Naturally, the high sensitivity to tuning poses a serious concern of the TMD. Due to mistuned frequency, the vibration suppression performance of the TMD will be impaired significantly, in practical terms, meaning that the TMD is not all robust.

In an attempt to remedy the narrow effective bandwidth of the TMD, one of the feasible alternatives is to employ the multiple tuned mass dampers (MTMD) with distributed natural frequencies which have been investigated by, for

*Corresponding author, Professor
E-mail: Li-chunxiang@vip.sina.com

ISSN: 2092-7614 (Print), 2092-7622 (Online)

example, Xu and Igusa (1992), Jangid (1995, 1999), Li (2000), Li and Liu (2003), Li and Qu (2006), Lin *et al*. (2010), Lin *et al*. (2010, 2017), Fu and Johnson (2011), Jokic *et al*. (2011), Li and Han (2011), Daniel *et al*. (2012), Li (2012), Mohebbi *et al*. (2013), Daniel and Lavan (2014), Dinh and Basu (2015), Leandro *et al*. (2016), Bozer and Özsarıyıldız (2018). These studies show that the MTMD can flatten the frequency response curve of a structure over the increasingly widened frequency range with the increase of the optimum frequency spacing through suppression of the secondary peaks induced by the MTMD by resorting to the larger optimum average damping ratio and/or the larger total number. Simultaneously, the semi-active tuned mass damper is seen to be a promising solution to the detuning problem of the TMD due to the unique feature that it in real-time updates the stiffness or damping of the TMD based on the sensed data on the actual vibration state of the structure. Moreover, the nonlinear tuned mass damper (NTMD) investigated by, for example, Sun *et al*. (2013), Eason *et al*. (2013), Luo *et al*. (2014), is also one of the feasible alternatives to overcome the above limitation. In comparison with the TMD, the NTMD is provided with the cubic stiffness nonlinearity rather than linear stiffness, thereby being capable of broadening the suppression bandwidth and providing a wider-band frequency-response amplitude reduction.

It has been above stated that the TMD is effective for the structures in the case of the long-distance narrow band earthquake excitations with long durations, namely the far-field (FF) earthquakes. Here lies in the explanation for this general recognition. The long-distance earthquake excitations are long-period (low frequency) motions with a predominant period closer to or longer than the natural period of the structure, usually produced by subduction faults or soft soil conditions. The long-distance earthquake excitations may result in large displacements in the structure due to resonance, thereby enabling one to regard base excitations of this kind as harmonic excitations. But the effectiveness of the TMD decreases as the input duration shortens. As a result, the effectiveness of the TMD is greatly less for near-fault (NF), especially pulse-like near-fault ground motion than for far-field (FF) one. The pulse-like NF ground motion includes the low-frequency component, broadband or high-frequency component, thus with the impulsive and multi-frequency characters. The pulse-like NF may result in large-amplitude, long-period pulses in the velocity and displacement time histories, which are particularly challenging for the structural safety of long-period structures. Therefore, in recent years, besides detuning, this challenging issue also has triggered the latest development of improving the performance of structures exposed to both the FF and NF ground motions using the TMD, such as studies by Lin *et al*. (2010), Matta (2013), Bekdas and Nigdeli (2013), Lucchini *et al*. (2014).

In order to confront such ground motions, a general observation is that the mass ratio of the TMD needs to be much higher (beyond 5%), since the TMD vibration control efficacy and robustness to detuning effects depend on its inertia property. The larger the attached TMD mass, the more effective the TMD will be. For seismically excited buildings, a large attached mass needs to be taken into account so as to achieve a satisfactory performance. Employing a large mass ratio boosts the cost of the TMD and simultaneously increases the weight of the structure, but contrary to increasing the seismic action. What’s more, in tall (low-frequency) buildings, the TMD requires occupying a large space, usually at a top floor, to accommodate the large displacement of the TMD mass block (i.e., the relative displacement of the TMD mass block with respect to its attachment point, called the stroke). Therefore, the mass ratio of the TMD must be kept in minimum levels for tall buildings. From here, we see that the requirement of a large mass ratio appeared to be a serious bottleneck in the TMD for controlling seismic vibrations of structures.

In order to surmount this large mass ratio restriction, a very promising alternative is to take advantage of the active tuned mass damper (ATMD) which have been investigated by, for example, Chang and Soong (1980), Chang and Yang (1995), Collins *et al*. (2006), Guclu and Yazici (2008), Li *et al*. (2010), Amini *et al*. (2013), Li and Cao (2015), Cao and Li (2018), to achieve better mitigation in the structural displacement and/or acceleration against the NF ground motions. The ATMD shares the advantages of the active control, needing a lower actuation power with respect to the purely active systems, with the capability of working as passive systems when power supply is missing. Due to applying a direct driving force, the ATMD remarkably enhances both the effectiveness and robustness of the TMD with a smaller mass ratio. Likewise, what is worth mentioning is that in order to design a structural seismic control system that is effective in reducing displacements while simultaneously decreasing accelerations, the ATMD is a cost-effective alternative. For super-tall buildings, however, in order to achieve the required levels of response reduction during moderate and strong earthquakes, while admitting that the ATMD may be taken into account, but a large control force must be created and simultaneously, a big mass ratio is needed. For the structures which permit behaving nonlinearly under large earthquakes, the ATMD simultaneously necessitates both high power and high mass ratio. Both the power limitation of actuator and the mass ratio restriction, taking physical and economic conditions into account, prevent this system from being implemented in such super-tall buildings. Evidently, it is imperative and of practical interest to seek for the control systems, which can simultaneously relax the requirements for masses and control forces delivered by actuators, and furthermore reduce the large stroke demand. The control system with this peculiar ability easily is implemented and thereby, reducing the capital and long-standing maintenance costs.

In the very last years, the light TMD through the incorporation of an inerter into a TMD, named the tuned mass damper inerter (TMDI), which may attain approximate or even better performances of the TMD, have been developed. The TMDI have been investigated by, for example, Marian and Giaralis (2014), Pietrosanti *et al*. (2017), Giaralis and Petrini (2017), Domenico and Ricciardi (2018), Giaralis and Taflanidis (2018). They concluded that the TMDI can lighten the weight of the TMD and improve

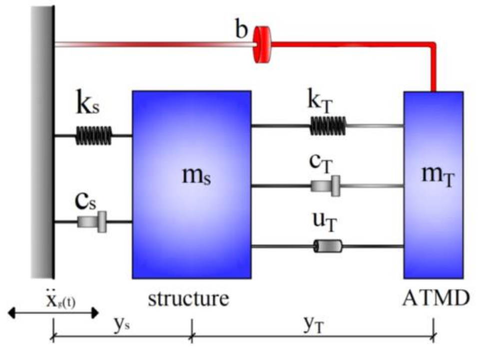

Fig. 1(a) Modeling of the SDOF structure-ATMDI system

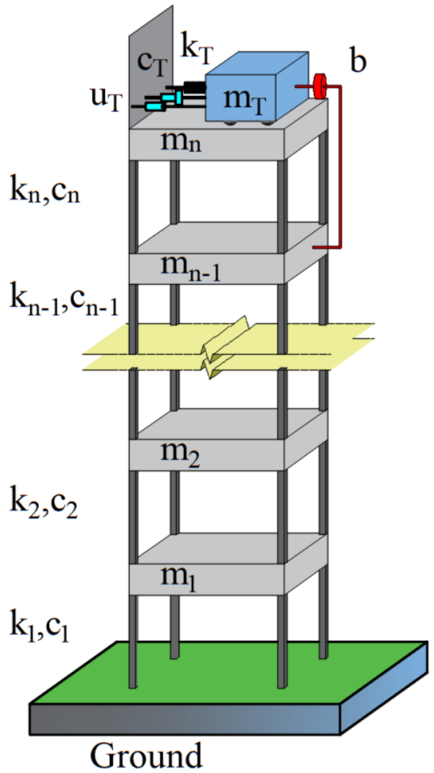

Fig. 1(b) Modeling of the MDOF structure-ATMDI system

its performance. Employing the inerter-based devices for structural vibration suppression has been a popular research topic since inerter's first introduction in 2002 (2002). The inerter is able to generate a resisting force, proportional to the relative acceleration of its terminals, equivalent to a force produced with an apparent (effective) mass two orders of magnitude greater than its own physical mass. The constant of proportionality of the inerter is called the inertance generated from the rotation of a flywheel; it has the dimension of a mass and fully characterizes the behavior of the device. Hitherto, there are three main types of inerter devices: rack and pinion inerter devices (2014), ball and screw inerter devices (2012), and hydraulic inerter devices (2010). When the inerter is installed in series with both the spring and damper elements, a lower-mass and more effective alternative to the traditional TMD is obtained, namely the TMDI, wherein the inertance plays the role of the TMD mass. Thus it can be seen that the TMDI is using the key feature of the inerter mass amplification effect that makes this device as a lower-mass alternative to a conventional TMD without increasing its weight. This is achieved by connecting the TMD mass via the inerter to a different floor from the one that the TMD is attached to in a multistory building (2017). Following the TMDI research, the active tuned mass damper-inerter have been proposed, referred to as the ATMDI in order to enhance the effectiveness of active tuned mass damper (ATMD) and solve the problem of its large stroke as well as further promote the miniaturization of the ATMD. The performances of the ATMDI will be investigated and demonstrated by extensive simulation results.

2. TFs of the structure-ATMDI system

Fig. 1(a) presents the modeling of the active tuned mass damper inerter (ATMDI) located on a single degree-of -freedom (SDOF) structure, effectively representing the mode generalized system in the specific vibration mode being controlled of the multi-degrees-of-freedom (MDOF) structures, excited by the ground acceleration [$\ddot{x}_g(t)$]. The present control system configuration contains both an ATMD and an inerter which links the ATMD mass block to the ground. The set of second-order differential equations of motion for the structure-ATMDI system can then be established as follows

$$m_s\left[\ddot{x}_g(t)+\ddot{y}_s\right]+c_s\dot{y}_s+k_s y_s-c_T\dot{y}_T-k_T y_T=-u_T(t) \tag{1}$$

$$m_T\left[\ddot{x}_g(t)+\ddot{y}_s+\ddot{y}_T\right]+c_T\dot{y}_T+k_T y_T=u_T(t)+f_I(t) \tag{2}$$

in which m_s and m_T are the mass of the structure and ATMDI, respectively; c_s and c_T represent the viscous damping coefficients of the structure and ATMDI, respectively; k_s and k_T refer to the stiffness coefficients of the structure and ATMDI, respectively; y_s and y_T denote the relative displacements of the structure and ATMDI with reference to their respective supports, that are the ground and structure, respectively; whereas $f_I(t)$ stands for the inerter element force which can be expressed as follows

$$f_I(t)=-b\left(\ddot{y}_s+\ddot{y}_T\right) \tag{3}$$

where b is the inertance coefficient measured in mass units. The function of the ideal inerter can be interpreted as an inertial weightless element whose gain depends on b and on the relative acceleration of its terminals.

And, $u_T(t)$ indicates the active control force generated by the actuators in the ATMDI system. Suppose that calculating the active control force of the ATMDI system in real time by resorting to feeding back the sensing signal can be written in a compact representation as follows

$$u_T(t)=-\bar{m}_T\ddot{y}_s-\bar{c}_T\dot{y}_T-\bar{k}_T y_T \tag{4}$$

where $\bar{m}_T$ indicates the gain of the ATMDI feeding back the acceleration of the structure; while $\bar{c}_T$ and $\bar{k}_T$

correspond, respectively, to the gains of feeding back the velocity and displacement of the ATMDI.

In order to render a compact formulation, we beforehand introduce the following new variables.

$a_s = \ddot{x}_g(t) + \ddot{y}_s$, $a_T = \ddot{x}_g(t) + \ddot{y}_s + \ddot{y}_T$, $\mu_T = \dfrac{m_T}{m_s}$, $\mu_I = \dfrac{b}{m_s}$,

$\alpha_T = \dfrac{\bar{m}_T}{m_T}$, $\omega_s = \sqrt{\dfrac{k_s}{m_s}}$, $\omega_T = \sqrt{\dfrac{k_T + \bar{k}_T}{m_T}}$, $\xi_s = \dfrac{c_s}{2m_s\omega_s}$,

$\xi_T = \dfrac{c_T + \bar{c}_T}{2m_T\omega_T}$

Laplace transforms of the displacement, velocity, acceleration responses, ground acceleration, active control force, and inerter element force are respectively defined as a set of Equations as follows:

$Y_s(s) = L[y_s(t)]$, $Y_T(s) = L[y_T(t)]$, $sY_s(s) = L[\dot{y}_s(t)]$, $sY_T(s) = L[\dot{y}_T(t)]$, $s^2Y_s(s) = L[\ddot{y}_s(t)]$, $s^2Y_T(s) = L[\ddot{y}_T(t)]$,

$A_s(s) = L[a_s(t)]$, $A_T(s) = L[a_T(t)]$,

$\ddot{X}_g(s) = L[\ddot{x}_g(t)]$, $U_T(s) = L[u_T(t)]$, $F_I(s) = L[f_I]$

Employing Eqs. (3) and (4) and the above Laplace transforms, then Eqs. (1) and (2) can be rewritten in the Laplace domain under the terms of displacement as follows

$$\ddot{X}_g(s) + \left[(1-\alpha_T\mu_T)s^2 + 2\xi_s\omega_s s + \omega_s^2\right] Y_s(s) - \left(2\mu_T\xi_T\omega_T s + \mu_T\omega_T^2\right)Y_T(s) = 0 \tag{5}$$

$$\ddot{X}_g(s) + \left(1 + \alpha_T + \frac{\mu_I}{u_T}\right)s^2Y_s(s) + \left[\left(1 + \frac{\mu_I}{u_T}\right)s^2 + 2\xi_T\omega_T s + \omega_T^2\right]Y_T(s) = 0 \tag{6}$$

where

$A_s(s) = \ddot{X}_g(s) + s^2Y_s(s)$, $A_T(s) = \ddot{X}_g(s) + s^2Y_s(s) + s^2Y_T(s)$

$U_T(s) = -\bar{m}_T s^2Y_s(s) - \bar{c}_T sY_T(s) - \bar{k}_T Y_T(s)$,

$F_I(s) = -b\left[s^2Y_s(s) + s^2Y_T(s)\right]$

By substituting $s=i\omega$ in Eqs. (5) and (6), where $i = \sqrt{-1}$, and through simultaneously solving Eqs. (5)-(6), the transfer functions in the Laplace domain of the structure with the attached ATMDI, active control force, and inerter element force can then be expressed in a compact form, respectively as below

For the displacement transfer function (DTF) of the structure with the ATMDI

$$\frac{Y_s(i\omega)}{\ddot{X}_g(i\omega)} = -\frac{C_{s2}(i\omega)^2 + C_{s1}(i\omega) + C_{s0}}{D_{s4}(i\omega)^4 + D_{s3}(i\omega)^3 + D_{s2}(i\omega)^2 + D_{s1}(i\omega) + D_{s0}} \tag{7}$$

For the displacement transfer function (DTF) of the ATMDI mass block

$$\frac{Y_T(i\omega)}{\ddot{X}_g(i\omega)} = -\frac{1 + B_2(i\omega)^2 \dfrac{Y_s(i\omega)}{\ddot{X}_g(i\omega)}}{B_3(i\omega)^2 + 2\xi_T\omega_T(i\omega) + \omega_T^2} \tag{8}$$

For the acceleration transfer function (ATF) of the structure with the ATMDI

$$\frac{A_s(i\omega)}{\ddot{X}_g(i\omega)} = 1 + \frac{(i\omega)^2 Y_s(i\omega)}{\ddot{X}_g(i\omega)} \tag{9}$$

For the active control force transfer function (ACF-TF) of the ATMDI

$$\frac{U_T(i\omega)}{m_s\ddot{X}_g(i\omega)} = -\mu_T\left[\alpha_T\frac{(i\omega)^2 Y_s(i\omega)}{\ddot{X}_g(i\omega)} + 2\left(\xi_T\omega_T - \xi_{TMDI}\omega_{TMDI}\right)(i\omega)\frac{Y_T(i\omega)}{\ddot{X}_g(i\omega)} + \left(\omega_T^2 - \omega_{TMDI}^2\right)\frac{Y_T(i\omega)}{\ddot{X}_g(i\omega)}\right] \tag{10}$$

For the inerter element force transfer function (IEF-TF) of the ATMDI

$$\frac{F_I(i\omega)}{m_s\ddot{X}_g(i\omega)} = -\mu_I(i\omega)^2\left(\frac{Y_s(i\omega)}{\ddot{X}_g(i\omega)} + \frac{Y_T(i\omega)}{\ddot{X}_g(i\omega)}\right) \tag{11}$$

in which

ω_{TMDI} and ξ_{TMDI} represent the natural frequency and damping ratio of the TMDI (i.e., the passive counterpart of the ATMDI), respectively

$B_1 = 1 - \alpha_T\mu_T$, $B_2 = 1 + \alpha_T + \dfrac{\mu_I}{u_T}$, $B_3 = 1 + \dfrac{\mu_I}{u_T}$

$C_{s2} = B_3$, $C_{s1} = 2(1+\mu_T)\xi_T\omega_T$, $C_{s0} = (1+\mu_T)\omega_T^2$

$D_{s4} = B_1B_3$, $D_{s3} = 2B_3\xi_s\omega_s + 2B_1\xi_T\omega_T + 2B_2\mu_T\xi_T\omega_T$

$D_{s2} = B_3\omega_s^2 + 4\xi_s\xi_T\omega_s\omega_T + B_1\omega_T^2 + B_2\mu_T\omega_T^2$,

$D_{s1} = 2\xi_T\omega_s^2\omega_T + 2\xi_s\omega_s\omega_T^2$, $D_{s0} = \omega_s^2\omega_T^2$

Further, Fig. 1(b) presents the modeling of the MDOF structure-ATMDI system. The ATMDI can be applied to mitigate the vibration of an MDOF structure. In this case, the ATMD need to be placed at the top floor of the structure, whereas the inerter is linked to one storey below the top floor or span more than one storey down.

3. DMFs of the structure-ATMDI system

Introducing the variables: $\lambda = \dfrac{\omega}{\omega_s}$ and $f_T = \dfrac{\omega_T}{\omega_s}$, after some transformation, the

Eqs. (7)-(11) take the following form.

$$\frac{\omega_s^2 Y_s(i\lambda)}{\ddot{X}_g(i\lambda)} = -\frac{\left(-C'_{s2}\lambda^2 + C'_{s0}\right) + \left(C'_{s1}\lambda\right)i}{\left(D'_{s4}\lambda^4 - D'_{s2}\lambda^2 + D'_{s0}\right) + \left(-D'_{s3}\lambda^3 + D'_{s1}\lambda\right)i} \tag{12}$$

$$\frac{\omega_s^2 Y_T(i\lambda)}{\ddot{X}_g(i\lambda)} = -\frac{1 + B_2(i\lambda)^2\dfrac{\omega_s^2 Y_s(i\lambda)}{\ddot{X}_g(i\lambda)}}{B_3(i\lambda)^2 + 2\xi_T f_T(i\lambda) + f_T^2} \tag{13}$$

$$\frac{A_T(i\lambda)}{\ddot{X}_g(i\lambda)} = 1 + \frac{(i\lambda)^2\omega_s^2 Y_s(i\lambda)}{\ddot{X}_g(i\lambda)} + \frac{(i\lambda)^2\omega_s^2 Y_T(i\lambda)}{\ddot{X}_g(i\lambda)} \tag{14}$$

$$\frac{U_T(i\lambda)}{m_s\ddot{X}_g(i\lambda)} = \alpha_T\mu_T\lambda^2\frac{\omega_s^2 Y_s(i\lambda)}{\ddot{X}_g(i\lambda)} - 2\mu_T(\xi_T f_T - \xi_{TMDI} f_{TMDI})\lambda\frac{\omega_s^2 Y_T(i\lambda)}{\ddot{X}_g(i\lambda)}i - \mu_T(f_T^2 - f_{TMDI}^2)\frac{\omega_s^2 Y_T(i\lambda)}{\ddot{X}_g(i\lambda)} \tag{15}$$

$$\frac{F_I(i\lambda)}{m_s\ddot{X}_g(i\lambda)}=\mu_I\lambda^2\left(\frac{\omega_s^2Y_s(i\lambda)}{\ddot{X}_g(i\lambda)}+\frac{\omega_s^2Y_T(i\lambda)}{\ddot{X}_g(i\lambda)}\right) \tag{16}$$

where

$C_{s2}^{'}=B_3$, $C_{s1}^{'}=2(1+\mu_T)\xi_T f_T$, $C_{s0}^{'}=(1+\mu_T)f_T^2$

$D_{s4}^{'}=B_1B_3$, $D_{s3}^{'}=2B_3\xi_s+2B_1\xi_T f_T+2B_2\mu_T\xi_T f_T$

$D_{s2}^{'}=B_3+4\xi_s\xi_T f_T+B_1 f_T^2+B_2\mu_T f_T^2$, $D_{s1}^{'}=2\xi_T f_T+2\xi_s f_T^2$,

$D_{s0}^{'}=f_T^2$

Employing the Eqs. (12)-(16), the dynamic magnification factors (DMF) of the structure-ATMDI system can be derived, as shown below.

For the displacement DMF of the structure with the ATMDI

$$\begin{aligned}DMF_{Y_s}&=\left|\omega_s^2\left[Y_s(i\lambda)/\ddot{X}_g(i\lambda)\right]\right|\\&=\sqrt{\left[\bar{R}_e(\lambda)\right]^2+\left[\bar{I}_m(\lambda)\right]^2}\Big/\sqrt{\left[R_e(\lambda)\right]^2+\left[I_m(\lambda)\right]^2}\end{aligned} \tag{17}$$

For the displacement DMF (used for evaluating the stroke) of the ATMDI mass block

$$\begin{aligned}DMF_{Y_T}&=\left|\omega_s^2\left[Y_T(i\lambda)/\ddot{X}_g(i\lambda)\right]\right|\\&=\sqrt{\left[\bar{R}_{eT}(\lambda)\right]^2+\left[\bar{I}_{mT}(\lambda)\right]^2}\Big/\sqrt{\left[R_{eT}(\lambda)\right]^2+\left[I_{mT}(\lambda)\right]^2}\end{aligned} \tag{18}$$

For the acceleration DMF of the structure with the ATMDI

$$\begin{aligned}DMF_{A_s}&=\left|\left[A_s(i\lambda)/\ddot{X}_g(i\lambda)\right]\right|\\&=\sqrt{\left[\bar{R}_{ea}(\lambda)\right]^2+\left[\bar{I}_{ma}(\lambda)\right]^2}\Big/\sqrt{\left[R_{ea}(\lambda)\right]^2+\left[I_{ma}(\lambda)\right]^2}\end{aligned} \tag{19}$$

For the active control force DMF of the ATMDI

$$\begin{aligned}DMF_{U_T}&=\left|\left[U_T(i\lambda)/m_s\ddot{X}_g(i\lambda)\right]\right|\\&=\sqrt{\left[\bar{R}_{eu}(\lambda)\right]^2+\left[\bar{I}_{mu}(\lambda)\right]^2}\Big/\sqrt{\left[R_{eu}(\lambda)\right]^2+\left[I_{mu}(\lambda)\right]^2}\end{aligned} \tag{20}$$

For the inerter element force DMF of the ATMDI

$$\begin{aligned}DMF_{F_I}&=\left|\left[F_I(i\lambda)/m_s\ddot{X}_g(i\lambda)\right]\right|\\&=\sqrt{\left[\bar{R}_{eI}(\lambda)\right]^2+\left[\bar{I}_{mI}(\lambda)\right]^2}\Big/\sqrt{\left[R_{eI}(\lambda)\right]^2+\left[I_{mI}(\lambda)\right]^2}\end{aligned} \tag{21}$$

where

$\bar{R}_e(\lambda)=-C_{s2}^{'}\lambda^2+C_{s0}^{'}$, $\bar{I}_m(\lambda)=C_{s1}^{'}\lambda$

$R_e(\lambda)=D_{s4}^{'}\lambda^4-D_{s2}^{'}\lambda^2+D_{s0}^{'}$, $I_m(\lambda)=-D_{s3}^{'}\lambda^3+D_{s1}^{'}\lambda$

$\bar{R}_{eT}(\lambda)=R_e(\lambda)+B_2\lambda^2\bar{R}_e(\lambda)$, $\bar{I}_{mT}(\lambda)=I_m(\lambda)+B_2\lambda^2\bar{I}_m(\lambda)$

$R_{eT}(\lambda)=\left(-B_3\lambda^2+f_T^2\right)R_e(\lambda)-2\xi_T f_T\lambda I_m(\lambda)$

$I_{mT}(\lambda)=\left(-B_3\lambda^2+f_T^2\right)I_m(\lambda)+2\xi_T f_T\lambda R_e(\lambda)$

$\bar{R}_{ea}(\lambda)=-\left[R_e(\lambda)+\lambda^2\bar{R}_e(\lambda)\right]$, $\bar{I}_{ma}(\lambda)=-\left[I_m(\lambda)+\lambda^2\bar{I}_m(\lambda)\right]$

$R_{ea}(\lambda)=R_e(\lambda)$, $I_{ma}(\lambda)=I_m(\lambda)$

$$\bar{R}_{eaT}(\lambda)=-\begin{bmatrix}R_e(\lambda)R_{eT}(\lambda)-I_m(\lambda)I_{mT}(\lambda)+\lambda^2\bar{R}_e(\lambda)R_{eT}(\lambda)-\lambda^2\bar{I}_m(\lambda)I_{mT}(\lambda)\\+\lambda^2\bar{R}_{eT}(\lambda)R_e(\lambda)-\lambda^2\bar{I}_{mT}(\lambda)I_m(\lambda)\end{bmatrix}$$

$$\bar{I}_{maT}(\lambda)=-\begin{bmatrix}R_e(\lambda)I_{mT}(\lambda)+I_m(\lambda)R_{eT}(\lambda)+\lambda^2\bar{R}_e(\lambda)I_{mT}(\lambda)+\lambda^2\bar{I}_m(\lambda)R_{eT}(\lambda)\\+\lambda^2\bar{R}_{eT}(\lambda)I_m(\lambda)+\lambda^2\bar{I}_{mT}(\lambda)R_e(\lambda)\end{bmatrix}$$

$R_{eaT}(\lambda)=R_e(\lambda)R_{eT}(\lambda)-I_m(\lambda)I_{mT}(\lambda)$,

$I_{maT}(\lambda)=R_e(\lambda)I_{mT}(\lambda)+I_m(\lambda)R_{eT}(\lambda)$

$\bar{R}_{eu}(\lambda)=\mu_T\left[\alpha_T\lambda^2\bar{R}_e(\lambda)R_{eT}(\lambda)-\alpha_T\lambda^2\bar{I}_m(\lambda)I_{mT}(\lambda)-PR_e(\lambda)+QI_m(\lambda)\right]$

$\bar{I}_{mu}(\lambda)=\mu_T\left[\alpha_T\lambda^2\bar{R}_e(\lambda)I_{mT}(\lambda)+\alpha_T\lambda^2\bar{I}_m(\lambda)R_{eT}(\lambda)-PI_m(\lambda)-QR_e(\lambda)\right]$

$R_{eu}(\lambda)=R_e(\lambda)R_{eT}(\lambda)-I_m(\lambda)I_{mT}(\lambda)$,

$I_{mu}(\lambda)=R_e(\lambda)I_{mT}(\lambda)+I_m(\lambda)R_{eT}(\lambda)$

$\bar{R}_{eI}(\lambda)=\mu_I\lambda^2\left[\bar{R}_e(\lambda)R_{eT}(\lambda)-\bar{I}_m(\lambda)I_{mT}(\lambda)+\bar{R}_{eT}(\lambda)R_e(\lambda)-\bar{I}_{mT}(\lambda)I_m(\lambda)\right]$

$\bar{I}_{mI}(\lambda)=-\mu_I\lambda^2\left[\bar{R}_e(\lambda)I_{mT}(\lambda)+\bar{I}_m(\lambda)R_{eT}(\lambda)+\bar{R}_{eT}(\lambda)I_m(\lambda)+\bar{I}_{mT}(\lambda)R_e(\lambda)\right]$

$R_{eI}(\lambda)=R_e(\lambda)R_{eT}(\lambda)-I_m(\lambda)I_{mT}(\lambda)$,

$I_{mI}(\lambda)=R_e(\lambda)I_{mT}(\lambda)+I_m(\lambda)R_{eT}(\lambda)$

$P=-2(\xi_T f_T-\xi_{TMDI}f_{TMDI})\lambda\bar{I}_{mT}(\lambda)+(f_T^2-f_{TMDI}^2)\bar{T}_{eT}(\lambda)$

$Q=-2(\xi_T f_T-\xi_{TMDI}f_{TMDI})\lambda\bar{R}_{eT}(\lambda)+(f_T^2-f_{TMDI}^2)\bar{I}_{mT}(\lambda)$

4. PSO-based searching of the ATMDI

The objective for the optimization of the ATMDI design parameters in this study is to reduce the maximum DMF of the controlled structure, with the objective function defined as the minimization of the maximum values of the DMF (Eq. (17)), which can be mathematically written as follows

$$R=\min.\max.DMF_{Y_S} \tag{22}$$

Through the minimization of the maximum values of the DMF of the structure equipped with the ATMDI, the optimum parameters, effectiveness, and stroke of the ATMDI are investigated to evaluate and compare its control performance. The optimum parameters of the ATMDI include both the optimum tuning ratio and optimum damping ratio. In the present work, a metaheuristic algorithm, namely the particle swarm optimization (PSO) (Clerc and Kennedy 2002, Kannan *et al*. 2009) is taken into consideration for the optimum search of the ATMDI by resorting to MATLAB software platform. Fig. 2 provides the implementation flowchart of the PSO-based searching of the ATMDI.

5. Estimating the performance of the ATMDI

The two variables (f_T and ξ_T) to be optimized as well as their respective incremental intervals (Δf_T and $\Delta\xi_T$) are listed in Table 1. The ratio of the inertance coefficient to the structural mass is known as the inerter mass ratio (μ_I). The α_T is the normalized acceleration feedback gain factors (NAFGF) of the ATMDI. In order to take into account the effect of the mass ratio (μ_T) on the ATMDI, its different values are singled out. And more importantly, in order to provide valuable insights into the sensitivity of the ATMDI to the inerter mass ratio, its diverse values are taken into consideration and served as the abscissa of the graphs, except for the frequency response plots. The nondimensional frequency of excitation (NFE) is regarded as a continuous variable in MATLAB code. The assigned values of μ_T, α_T, and the modal damping ratio of structures (ξ_S) are presented in Table 1. For the sake of comparison, the optimum results of the ATMD (i.e., the special case of

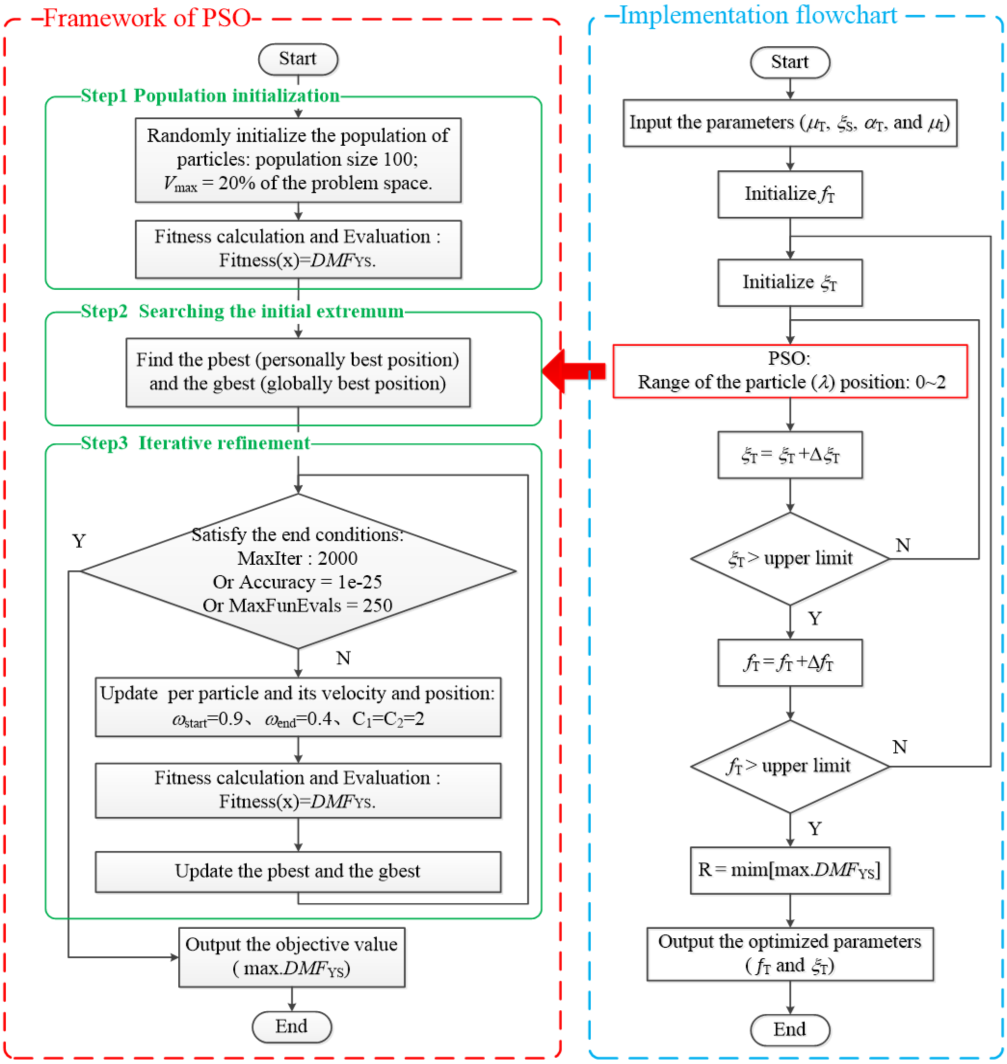

Fig. 2 Framework of PSO based searching of the ATMDI

Table 1 Targets and ranges of explored parameters as well as assigned parameter values

f_T (to be optimized)	$0 \le f_T \le 10$	Δf_T=0.001
ξ_T (to be optimized)	$0 \le \xi_T \le 0.999$	$\Delta\xi_T$=0.001
Mass ratio: μ_T=0.01, 0.005, 0.0025		
NAFGF: α_T=2, 4, 6, 8		
Inerter mass ratio: μ_I=0, 0.01, 0.02, 0.03, 0.04, 0.05		
NFE: $0 \le \lambda \le 2$		

the ATMDI with μ_I=0), and the TMDI (i.e., the special case of the ATMDI with α_T=0) are simultaneously included into consideration. The PSO-based minimization of Equation (22) will lead to the optimal parameters of the ATMDI system. Likewise, the lower the value of the objective function, the higher the effectiveness of the ATMDI. Herein, it is especially pointed out that in the following graphs, R denotes the minimization of the maximum values of the DMF of the structure coupled with the ATMDI; f_{Topt} and ξ_{Topt} represent the optimum tuning frequency ratio and the optimum damping ratio of the ATMDI; max.DMF_{A_s} is the maximum value of the acceleration DMF of the structure installed with the ATMDI taking its respective optimum parameters; and max.DMF_{Y_T}, max.DMF_{U_T}, and max.DMF_{F_I} respectively express the maximum value of the displacement DMF of the mass block, active control force DMF, and inerter element force DMF of the ATMDI taking its respective optimum parameters. It is pointed further that R is used to measure the effectiveness of the ATMDI, while max.DMF_{Y_T} is harnessed to evaluate the magnitude of the strokes of the ATMDI. By resorting to both the objective function and the PSO, the numerical results of R, max.DMF_{A_s}, max.DMF_{Y_T}, max.DMF_{U_T}, max.DMF_{F_I}, and the optimum parameters will be exhibited and analyzed next in detail.

5.1 Displacement control effectiveness

The plot of the variation tendency of R utilized for measuring the displacement control effectiveness of the ATMDI versus the inerter mass ratio is displayed in Fig. 3 with several important parameters. It can been seen from Fig. 3 that under the circumstances of the same mass ratio

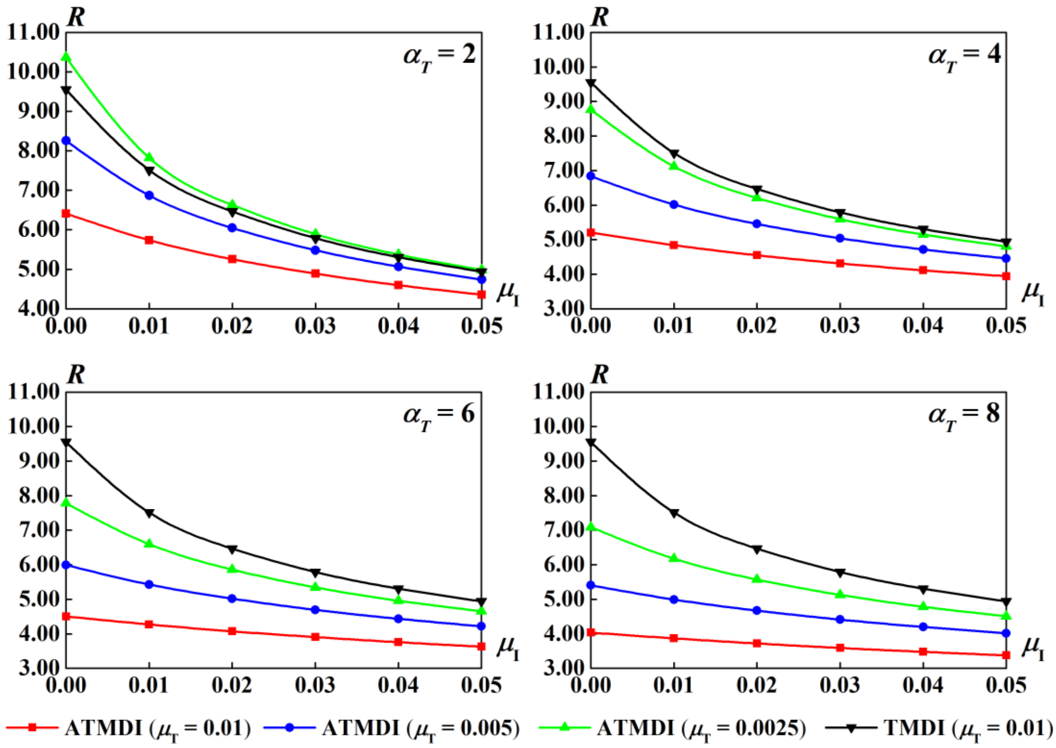

Fig. 3 Variation trends of *R* used for measuring the effectiveness of the ATMDI with reference to inerter mass ratio under the circumstances of several mass ratio and NAFGF values

and NAFGF value, the effectiveness of the ATMDI is remarkably better than that of the ATMD, indicating that the inerter can significantly enhance the displacement control effectiveness of the ATMD. The explanation for this phenomenon is that adding the inerter is equivalent to increasing the virtual mass *b* to the physical mass of the ATMD and then the ATMD inertia is greatly promoted yet without increasing its physical mass, thereby gaining the high effectiveness ATMDI system. Through scrutinizing the Fig. 3, the indepth demonstrations can be provided in the following. The values of *R* decrease but the decrease rate tends to reduce with the increasing of the mass ratio, NAFGF, and inerter mass ratio. The smaller the mass ratio of the ATMDI, the more obvious the change in the values of R with the inerter mass ratio. Therefore, the smaller the ATMDI mass block, the more significant the inerter mass amplification effect. However, when the inerter mass ratio is beyond 0.04, the further improvement in the effectiveness of the ATMDI is insignificant. That is to say the inertia function of the ATMDI system tends to be saturated with the inerter mass ratio beyond 0.04. Hence, the economic values of the inerter mass ratio are within the range from 0.01 to 0.04. The larger the NAFGF of the ATMDI, the less obvious the change in the values of R with the inerter mass ratio. This effectively indicates that an excessive active control force not only brings about some technical difficulties but also weakens the inerter mass amplification effect. Therefore, the economic values of NAFGF are suggested to be within the range from 2.0 to 6.0.

Combined with Table 2, the advantages of the ATMDI are summarized in the following. In the case of the same mass ratio and inerter mass ratio, the effectiveness of the

Table 2 Practically same level of effectiveness with different mass ratio, NAFGF, and inerter mass ratio

	μ_T	α_T	μ_I	R
TMDI	0.01	0	0.0425	5.2026
ATMD	0.01	4	0	5.2027
ATMDI	0.01	2	0.0212	5.2036
	0.005	2	0.0364	5.2027
		4	0.0258	5.2014
		6	0.0151	5.2040
		8	0.0045	5.2026
	0.0025	2	0.0440	5.2030
		4	0.0387	5.2018
		6	0.0334	5.2012
		8	0.0281	5.2005

ATMDI is remarkably higher than that of the ATMD. Although greatly reducing the mass block amplitude, the effectiveness of the ATMDI is yet obviously higher than that of the ATMD with a larger mass ratio. Employing the ATMDI can thus further miniaturize both the ATMD and TMDI. Under the circumstances of the practically same level of effectiveness, with respect to the TMDI, the ATMDI requires the obviously smaller mass ratio and inerter mass ratio, thus avoiding the difficulty of connecting the inerter due to the large inerter element force.

5.2 Acceleration control effectiveness

Fig. 4 presents the variation trends of max.DMF_{A_s} used for measuring the acceleration control effectiveness of the

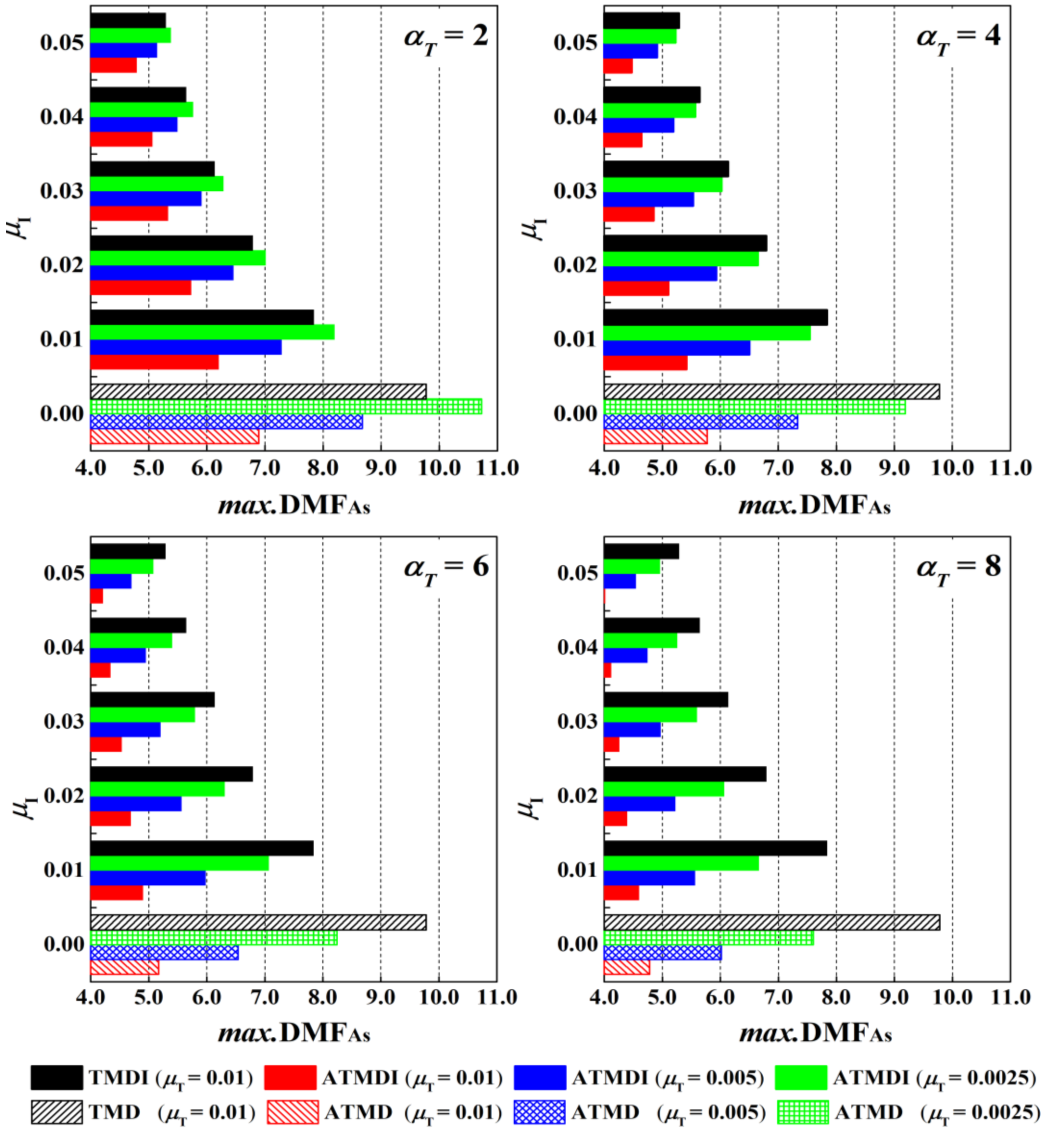

Fig. 4 Variation trends of max.DMF_{A_s} used for measuring the acceleration control effectiveness of the ATMDI with reference to inerter mass ratio under the circumstances of several mass ratio and NAFGF values

ATMDI with reference to the inerter mass ratio in the case of several mass ratio and NAFGF values. Let us be clear: the max.DMF_{A_s} value is calculated out using the optimum parameters obtained based upon the objective function (Eq. (22)). Fig. 4 clearly shows that when keeping the equal mass ratio, the ATMDI and TMDI may render the higher effectiveness in reducing the acceleration response with reference to the ATMD and TMD, respectively; in particular, the acceleration control effectiveness of the ATMDI is notably better than that of the TMDI and this advantage is more prominent with increasing in the NAFGF. Although greatly reducing the mass ratio, the effectiveness of the ATMDI is yet obviously higher than that of the TMDI with a larger mass ratio, thus indicating that the ATMDI can further miniaturize both the ATMD and TMDI and is applicable for the acceleration response mitigation of super-tall buildings.

5.3 Assessment of stroke

Fig. 5 clearly depicts the variation trends of max.DMF_{Y_T} employed for measuring the stroke of the ATMDI with reference to the inerter mass ratio under the circumstances of several mass ratio and NAFGF values. It can be identified from Fig. 5 that the strokes of both the ATMDI and TMDI are respectively smaller than those of both the ATMD and TMD and this merit is more prominent with increasing in the inerter mass ratio. But, this reduction in the stroke of the ATMDI tends to be saturated with the inerter mass ratio being beyond 0.04. Especially, in the context of a very small mass ratio, such as 0.0025, the ATMDI still keeps nearly the same stroke as the TMDI with a larger mass ratio, such as 0.01, with the inerter mass ratio being beyond 0.02. Furthermore, the stroke of the ATMDI is, by and large, insensitive to the NAFGF values. Based on the above elucidation of the stroke, the inerter mass ratio of the ATMDI is thus suggested to be within the range from 0.02 to 0.04.

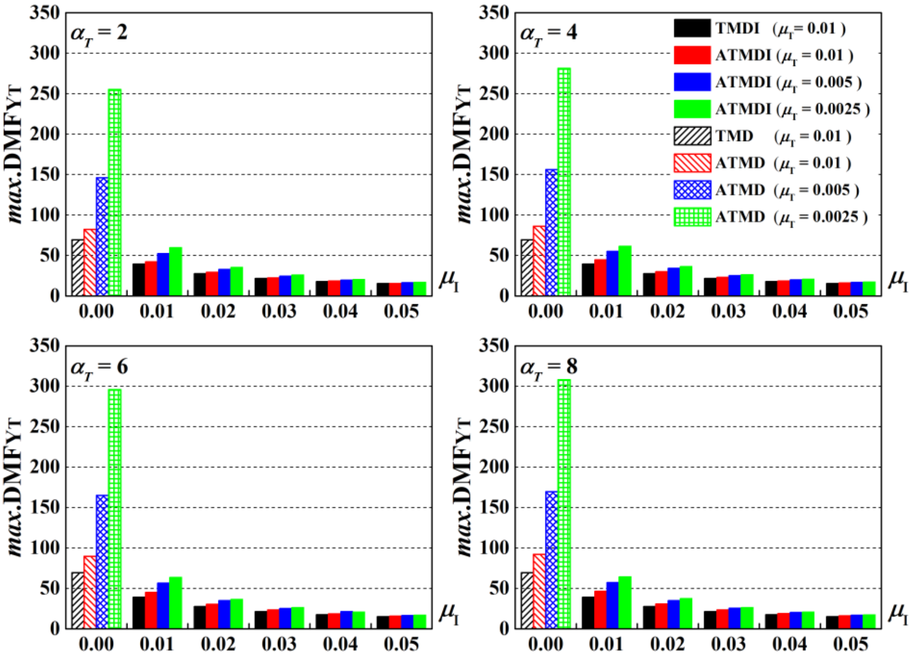

Fig. 5 Variation trends of max.DMF_{Y_T} used for measuring the stroke of the ATMDI with reference to inerter mass ratio under the circumstances of several mass ratio and NAFGF values

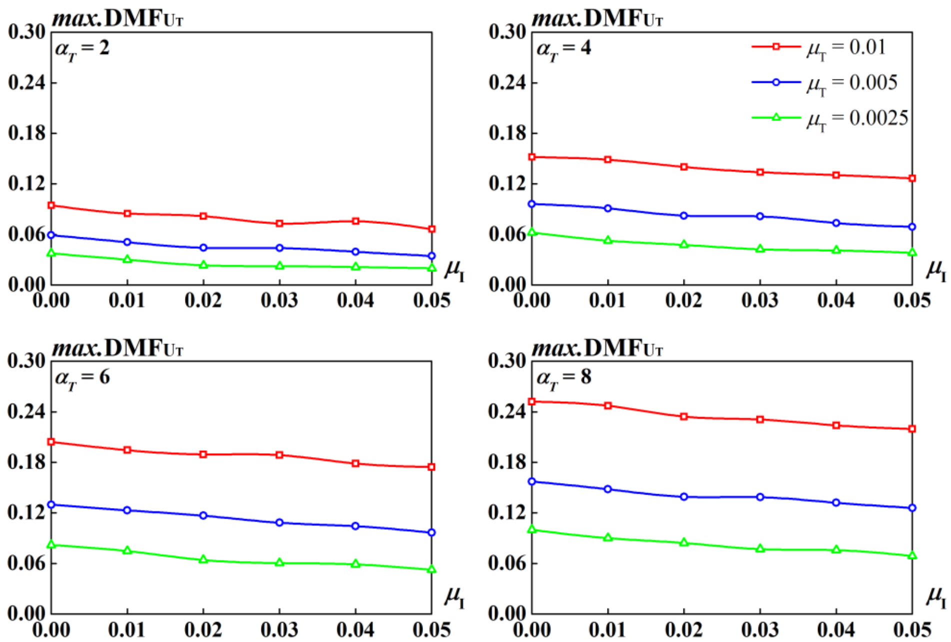

Fig. 6 Variation trends of max.DMF_{U_T} used for measuring the active control force of the ATMDI with reference to inerter mass ratio under the circumstances of several mass ratio and NAFGF values

5.4 Active control force and inerter element force

The graph of the variation trends of max.DMF_{U_T} with regard to the inerter mass ratio is presented in Fig. 6 utilized for measuring the active control force magnitude of the ATMDI. From Fig. 6, it can be clearly perceived that regardless of the mass ratio, the active control force of the ATMDI mildly decreases with the increase of the inerter mass ratio. Likewise, increasing both the mass ratio and NAFGF values leads to the demand of a larger active control force.

The variation trends of max.DMF_{F_I} used for measuring the inerter element force magnitude of the ATMDI with reference to the inerter mass ratio are compared in Fig. 7 under the circumstances of several mass ratio and NAFGF values and can be summarized as follows: (1) The inerter element force of the ATMDI is insensitive to the active control force and larger than that of the TMDI. (2) The inerter element force of the ATMDI increases with increasing in the inerter mass ratio. (3) The inerter element force of the ATMDI can be increased by decreasing the

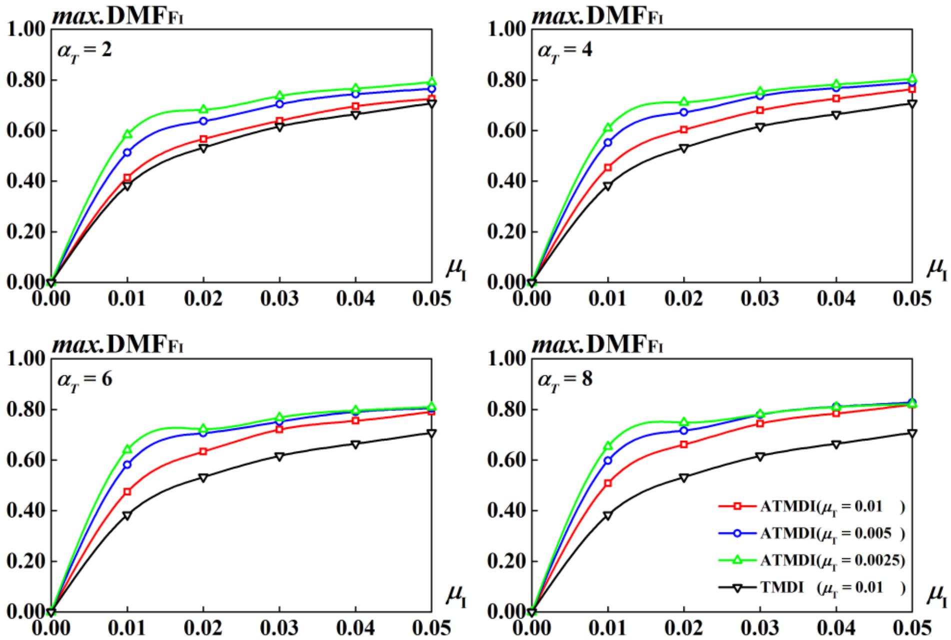

Fig. 7 Variation trends of max.DMF_{F_I} used for measuring the inerter element force of the ATMDI with reference to inerter mass ratio under the circumstances of several mass ratio and NAFGF values

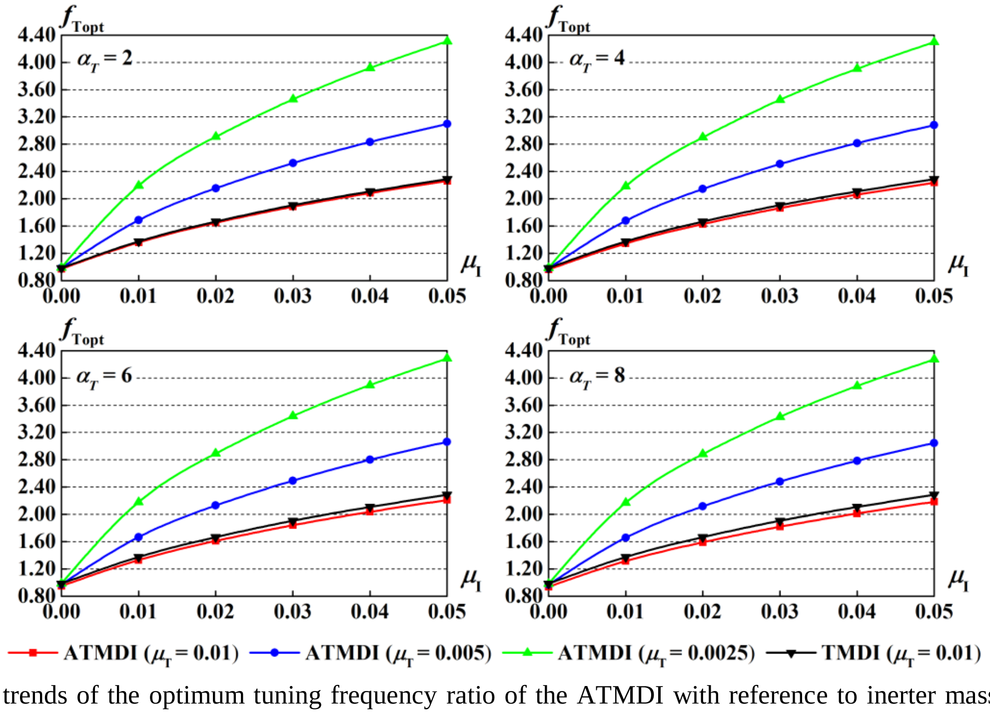

Fig. 8 Variation trends of the optimum tuning frequency ratio of the ATMDI with reference to inerter mass ratio under the circumstances of several mass ratio and NAFGF values

mass ratio, but not significantly, especially for a very small mass ratio, such as 0.005 and 0.0025.

5.5 Optimum parameter analysis

The **v**ariation trends of both the optimum tuning frequency ratio and damping ratio of the ATMDI with reference to the inerter mass ratio are presented, respectively, in Figs. 8 and 9 under the circumstances of several mass ratio and NAFGF values, and are briefly assessed as follows: (1) The optimum tuning frequency ratio of the ATMDI increases with increasing in the inerter mass ratio and decreasing in the mass ratio and is insensitive to the active control force. (2) It is interesting to note that regardless of both the inerter mass ratio and NAFGF, given the same mass ratio, such as 0.01, the ATMDI and TMDI have practically the same optimum tuning frequency ratio. (3) The optimum damping ratio of the ATMDI increases with increasing in the inerter mass ratio and decreasing in the mass ratio and is larger than that

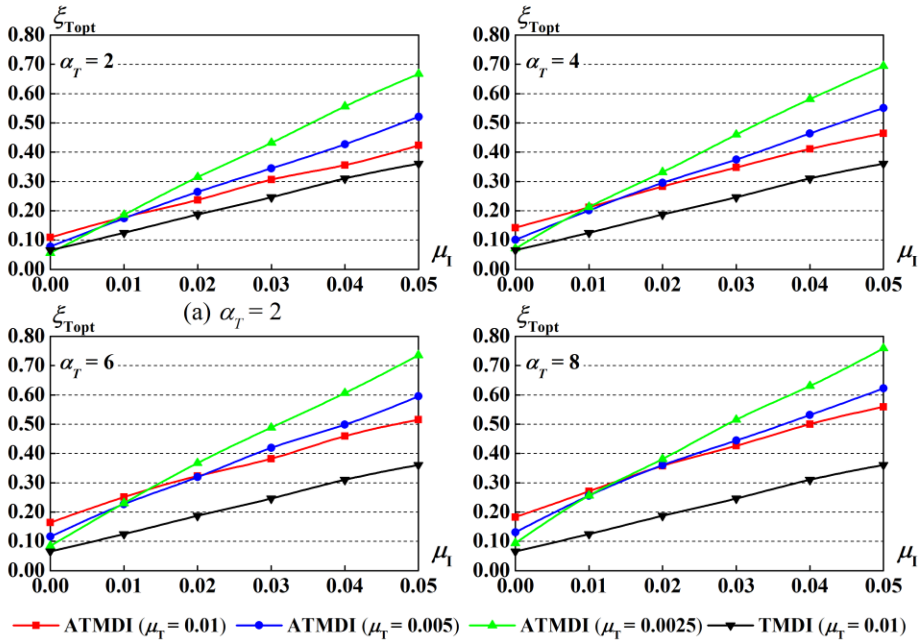

Fig. 9 Variation trends of the optimum damping ratio of the ATMDI with respect to inerter mass ratio under the circumstances of several mass ratio and NAFGF values

Table 3 Further comparison of optimum tuning frequency and damping ratios of both the ATMDI and TMDI at nearly identical level of effectiveness

	μ_T	α_T	μ_I	f_{Topt}	ξ_{Topt}	R
TMDI	0.01		0.05	2.287	0.361	4.938
ATMDI	0.01	2	0.03	1.883	0.306	4.891
		4	0.01	1.344	0.212	4.841
		6	0.01	1.328	0.251	4.271
	0.005	6	0.02	2.130	0.319	5.018
		8	0.01	1.657	0.256	4.992

of the TMDI. (4) In general, the active control force has little impact on the optimum damping ratio of the ATMDI.

Table 3 renders further comparison of the optimum tuning frequency and damping ratios of both the ATMDI and TMDI at nearly identical level of effectiveness. In this comparison, it is a pleasure to discover that at nearly identical level of effectiveness, the optimum tuning frequency and damping ratios, as well as the corresponding inerter mass ratio of the ATMDI are smaller than those of the TMDI in the optimum scenarios.

5.6 Frequency response of the controlled structure

The aim of Fig. 10 is to reveal the status that the optimum ATMDI, ATMD, and TMDI affect the max.DMF_{Y_S} (frequency response) curves of the controlled structure. Fig. 10 clearly depicts that the max.DMF_{Y_S} curves of the controlled structure attain two local maxima of equal height at two nondimensional frequencies of excitation (NFE), including the smaller and larger NFE, whose locations depend on both the inerter mass ratio and NAFGF. The nondimensional frequency range between the smaller and larger NFE is named the suppression bandwidth. In terms of Fig. 10, the optimum ATMDI, ATMD, and TMDI all can flatten the max.DMF_{Y_S} curves of the controlled structure, which means that the vibration mitigation can be achieved over a wider suppression bandwidth. Therefore, the control system which brings the wider suppression bandwidth will render better robustness. At the approximately equal level of effectiveness, the comparison among the variations trends in the max.DMF_{Y_S} curves of the controlled structure in the first row of Fig. 10 brings the following findings.

Although adopting a remarkably smaller inerter mass ratio with respect to the TMDI or a significantly smaller active control force with regard to the ATMD, the ATMDI may gain the nearly equal suppression bandwidth in the case of the same mass ratio. Further, the practically equal suppression bandwidth can be actualized making use of the ATMDI with a very small mass ratio and a very small inerter mass ratio or their different combinations.

The second row of Fig. 10 exhibits the variation trends in max.DMF_{Y_S} of the structure, respectively, equipped with the optimum ATMDI, ATMD, and TMDI with respect to NFE in consideration of changing several important parameters. From the second row of Fig. 10, it can be clearly seen that with the increase of the inerter mass ratio, the smaller and larger NFE values all decrease; but the rate of decline in the smaller NFE is greater than that of the larger one. More importantly, with the increase of the NAFGF values, the smaller and larger NFE values all increase, effectively meaning that the max.DMF_{Y_S} curves of the ATMDI are flatter than those of both the ATMD and TMDI. From here we see that the suppression bandwidth of the ATMDI is wider than that of both the ATMD and TMDI and may be further widened through increasing the inerter mass ratio and/or active control force. Therefore, the proposed ATMDI possesses better robustness (i.e., higher

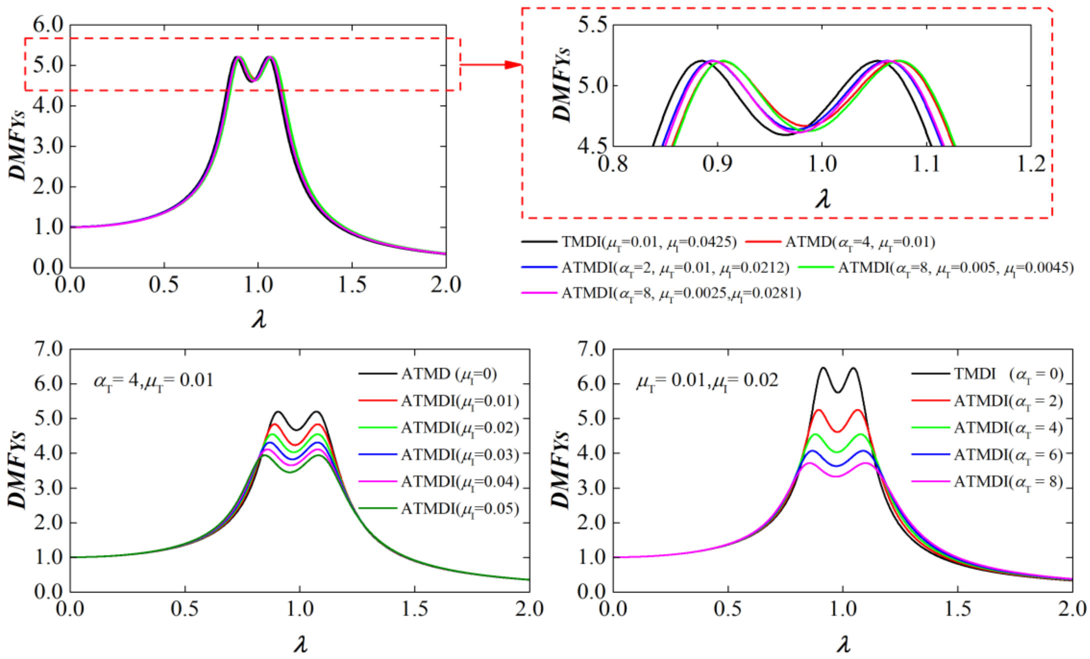

Fig. 10 Variation trends in max.DMF_{Y_S} of the structure respectively equipped with the optimum ATMDI, ATMD, and TMDI with respect to the NFE values

robustness against the change or the estimation error in the structural natural frequency) than both the ATMD and TMDI. Distinctly, in the suppression bandwidth, the effectiveness of the ATMDI is remarkably higher than that of the TMDI.

6. Conclusions

The ATMDI has been proposed to attenuate undesirable oscillations of structures under the ground acceleration. Owing to the high performance and the markedly light advantage, it is expected that the proposed ATMDI will be widely used in the future for the control of undesirable oscillations of super-tall buildings subjected to large earthquakes. From the results presented, the following conclusions can be drawn:

(1) Keeping the equal mass ratio and inerter mass ratio, the effectiveness of the ATMDI is remarkably higher than that of the ATMD. Although greatly reducing the mass block, the effectiveness of the ATMDI is yet obviously higher than that of both the ATMD and TMDI with a large mass ratio, thus indicating that the ATMDI can further miniaturize both the ATMD and TMDI.

(2) At nearly identical level of effectiveness, the ATMDI requires the obviously smaller mass ratio and inerter mass ratio with respect to the TMDI, thus avoiding the difficulty of connecting the inerter due to a large inerter element force.

(3) Although taking minimizing the maximum values of the displacement DMF of the controlled structure as the goal, the ATMDI can significantly reduce the structural acceleration response. Likewise, the effectiveness of the ATMDI is higher than that of the ATMD and remarkably higher than that of the TMDI.

(4) In the context of a very small mass ratio, the ATMDI still keeps nearly the same stroke as the TMDI with a larger mass ratio with the inerter mass ratio being beyond 0.02. Hence, the micro ATMDI has a smaller stroke, being suitable for the vibration mitigation of super-tall buildings.

(5) The suppression bandwidth of the ATMDI is wider than that of both the ATMD and TMDI and may be further widened through increasing the inerter mass ratio and/or active control force, demonstrating the ATMDI possesses better robustness than both the ATMD and TMDI.

(6) Based on the considerations of both the effectiveness and stroke, the inerter mass ratio of the ATMDI is thus suggested to be within the range from 0.02 to 0.04. Likewise, the economic values of NAFGF are within the range from 2.0 to 6.0.

In closing, based on the above conclusions, it can be asserted that the ATMDI is a high performance vibration control device and thus has a good application prospect. In the present paper, the performances of ATMDI have been investigated and demonstrated by extensive simulation results in the frequency domain. Surely, further investigations may be carried out with a focus on the performance evaluation of the ATMDI by using the frequency-dependent power spectral density (PSD) functions of earthquake ground motions, which are modeled as filtered Gaussian white noise processes, e.g., Tajimi-Kanai PSD function and Clough-Penzien PSD function, corresponding to a modification of Tajimi-Kanai PSD function. Likewise, these two models have been widely used for studying the vibration control systems of structures (e.g., Li and Liu 2004, and Anajafi and Medina 2018). Also, there is a need of implementing numerical simulations in the time domain using a three-dimensional model of super-tall buildings subjected to actual and artificial earthquake records in order to further conduct the performance assessment on the ATMDI. These will be discussed in a forthcoming paper by the authors.

References

Amini, F., Hazaveh, N.K. and Rad, A.A. (2013), "Wavelet PSO-based LQR algorithm for optimal structural control using active tuned mass dampers", *Comput. Aid. Civil Inf. Eng.*, **28**(7), 542-557.

Anajafi, C.H. and Medina, R.A. (2018), "Robust design of a multi-floor isolation system", *Struct. Control Hlth. Monit.*, **25**(4), e2130.

Bekdaş, G. and Nigdeli, S.M. (2013), "Mass ratio factor for optimum tuned mass damper strategies", *Int. J. Mech. Sci.*, **71**, 68-84.

Bozer, A. and Özsarıyıldız, Ş.S. (2018), "Free parameter search of multiple tuned mass dampers by using artificial bee colony algorithm", *Struct Control Hlth. Monit.*, **25**(2), e2066.

Cao, L. and Li, C. (2018), "Enhanced hybrid active tuned mass dampers for structures", *Struct. Control Hlth. Monit.*, **25**, e2067.

Casciati, F. and Giuliano, F. (2009), "Performance of Multi-TMD in the towers of suspension bridges", *J. Vib. Control,* **15**(6), 821-847.

Chang, C.C. and Yang, H.T.Y. (1995), "Control of buildings using active tuned mass dampers", *J. Eng. Mech*., ASCE, **121**(3), 355-366.

Chang, J.C.H. and Soong, T.T. (1980), "Structural control using active tuned mass damper", *J. Eng. Mech.*, ASCE, **106**(6), 1091-1098.

Chung, L.L., Wu, L.Y., Yang, C.S.W., Lien, K.H., Lin, M.C. and Huang, H.H. (2013), "Optimal design formulas for viscous tuned mass dampers in wind-excited structures", *Struct. Control Hlth. Monit.*, **20**(3), 320-336.

Clerc, M. and Kennedy, J. (2002), "The particle swarm-explosion, stability, and convergence in a multidimensional complex space", *IEEE Tran. Evol. Comput.*, **61**, 58-73.

Collins, R., Basu, B. and Broderick, B. (2006), "Control strategy using bang-bang and minimax principle for FRF with ATMDs", *Eng. Struct.*, **28**(3), 349-356.

Daniel, Y. and Lavan, O. (2014), "Gradient based optimal seismic retrofitting of 3D irregular buildings using multiple tuned mass dampers", *Comput. Struct*., **139**, 84-97.

Daniel, Y., Lavan, O. and Levy, R. (2012), "Multiple-tuned mass dampers for multimodal control of pedestrian bridges", *J. Struct. Eng.*, ASCE, **138**(9), 1173-1178.

Dinh, V.N. and Basu, B. (2015), "Passive control of floating offshore wind turbine nacelle and spar vibrations by multiple tuned mass dampers", *Struct. Control Hlth. Monit*., **22**(1), 152-176.

Domenico, D.D. and Ricciardi, G. (2018), "An enhanced base isolation system equipped with optimal tuned mass damper inerter (TMDI)", *Earthq. Eng. Struct. Dyn.*, **47**(5), 1169-1192.

Eason, R.P., Sun, C., Dick, A.J. and Nagarajaiah, S. (2013), "Attenuation of a linear oscillator using a nonlinear and a semi-active tuned mass damper in series", *J. Sound Vib*., **332**(1), 154-166.

Fadel Miguel, L.F., Lopez, R.H., Miguel, L.F.F. and Torii, A.J. (2016), "A novel approach to the optimum design of MTMDs under seismic excitations", *Struct. Control Hlth. Monit*., **23**(11), 1290-1313.

Fu, T.S. and Johnson, E.A. (2011), "Distributed mass damper system for integrating structural and environmental controls in buildings", *J. Eng. Mech.*, ASCE, **137**(3), 205-213.

Giaralis, A. and Petrini, F. (2017), "Wind-induced vibration mitigation in tall buildings using the tuned mass-damper-inerter", *J. Struct. Eng.*, ASCE, **143**(9), 04017127.

Giaralis, A. and Taflanidis, A.A. (2018), "Optimal tuned mass-damper-inerter (TMDI) design for seismically excited MDOF structures with model uncertainties based on reliability criteria", *Struct. Control Hlth. Monit*., **25**, e2082.

Guclu, R. and Yazici, H. (2008), "Vibration control of a structure with ATMD against earthquake using fuzzy logic controllers", *J. Sound Vib*., **318**(1-2), 36-49.

Ikago, K., Saito, K. and Inoue, N. (2012), "Seismic control of single-degree-of-freedom structure using tuned viscous mass damper", *Earthq. Eng. Struct. Dyn*., **41**(3), 463-474.

Jangid, R.S. (1995), "Dynamic characteristics of structures with multiple tuned mass dampers", *Struct. Eng. Mech.*, **3**(5), 497-509.

Jangid, R.S. (1999), "Optimum multiple tuned mass dampers for base-excited undamped system", *Earthq. Eng. Struct. Dyn.*, **28**(9), 1041-1049.

Jokic, M., Stegic, M. and Butkovic, M. (2011), "Reduced-order multiple tuned mass damper optimization: A bounded real lemma for descriptor systems approach", *J. Sound Vib*., **330**(22), 5259-5268.

Kannan, S.M., Sivasubramanian, R. and Jayabalan, V. (2009), "Particle swarm optimization for minimizing assembly variation in selective assembly", *Int. J. Adv. Manuf. Technol*., **42**(7-8), 793-803.

Lazar, I.F., Neild, S.A. and Wagg, D.J. (2014), "Using an inerter-based device for structural vibration suppression, *Earthq. Eng. Struct. Dyn*., **43**(8), 1129-1147.

Li, C. (2000), "Performance of multiple tuned mass dampers for attenuating undesirable oscillations of structures under the ground acceleration", *Earthq. Eng. Struct. Dyn*., **29**(9), 1405-1421.

Li, C. (2012), "Effectiveness of the active multiple tuned mass dampers for asymmetric structures considering soil-structure interaction effects", *Struct Des. Tall Spec. Build.*, **21**(8), 543-565.

Li, C. and Cao, B. (2015), "Hybrid active tuned mass dampers for structures under the ground acceleration", *Struct. Control Hlth. Monit*., **22**(4), 757-773.

Li, C. and Han, B. (2011), "Effect of dominant ground frequency and soil on multiple tuned mass dampers", *Struct Des. Tall Spec. Build.*, **20**(2), 151-163.

Li, C. and Liu, Y. (2003), "Optimum multiple tuned mass dampers for structures under ground acceleration based on the uniform distribution of system parameters", *Earthq. Eng. Struct. Dyn*., **32**(5), 671-690.

Li, C. and Liu, Y. (2004), "Ground motion dominant frequency effect on the design of multiple tuned mass dampers", *J. Earthq. Eng*., **8**(1), 89-105.

Li, C. and Qu, W. (2006), "Optimum properties of multiple tuned mass dampers for reduction of translational and torsional response of structures subject to ground acceleration", *Eng. Struct*., **28**(4), 472-494.

Li, C., Li, J. and Qu, Y. (2010), "An optimum design methodology of active tuned mass damper for asymmetric structures", *Mech. Syst. Signal Pr*., **24**(3), 746-765.

Lin, C.C., Chen, C.L. and Wang, J.F. (2010), "Vibration control of structures with initially accelerated passive tuned mass dampers under near-fault earthquake excitation", *Comput. Aid. Civil Inf. Eng*., **25**(1), 69-75.

Lin, C.C., Lin, G.L. and Chiu, K.C. (2017), "Robust design strategy for multiple tuned mass dampers with consideration of frequency bandwidth", *Int. J. Struct. Stab. Dyn*., **17**(1), 1750002.

Lin, C.C., Lu, L.Y., Lin, G.L. and Yang, T.W. (2010), "Vibration control of seismic structures using semi-active friction multiple tuned mass dampers", *Eng. Struct.*, **32**(10), 3404-3417.

Lin, C.C., Wang, J.F., Lien, C.H., Chiang, H.W. and Lin, C.S. (2010), "Optimum design and experimental study of multiple tuned mass dampers with limited stroke", *Earthq. Eng. Struct. Dyn.*, **39**(14), 1631-1651.

Lu, X. and Chen, J. (2011), "Mitigation of wind-induced response of Shanghai Center Tower by tuned mass damper", *Struct Des. Tall Spec Build.*, **20**(4), 435-452.

Lu, X. and Chen, J. (2011), "Parameter optimization and structural design of tuned mass damper for Shanghai centre tower", *Struct Des. Tall Spec. Build.*, **20**(4), 453-471.

Lucchini, A., Greco, R., Marano, G. and Monti, G. (2014), "Robust design of tuned mass damper systems for seismic protection of multistory buildings", *J. Struct. Eng.*, ASCE, **140**(8), A4014009.

Luo, J., Wierschem, N., Fahnestock, L., Bergman, L., Spencer, Jr. B., AL-Shudeifat, M., McFarland, D., Quinn, D. and Vakakis, A. (2014), "Realization of a strongly nonlinear vibration mitigation device using elastomeric bumpers", *J. Eng. Mech.*, ASCE, **140**(5), 1-11.

Marian, L. and Giaralis, A. (2014), "Optimal design of a novel tuned mass-damper-inerter (TMDI) passive vibration control configuration for stochastically support-excited structural systems", *Prob. Eng. Mech.*, **38**, 156-164.

Matta, E. (2013), "Effectiveness of tuned mass dampers against ground motion pulses", *J. Struct. Eng.*, ASCE, **139**(2), 188-198.

Mohebbi, M., Shakeri, K., Ghanbarpour, Y. and Majzoub, H. (2013), "Designing optimal multiple tuned mass dampers using genetic algorithms (GAs) for mitigating the seismic response of structures", *J. Vib. Control*, **19**(4), 605-625.

Pietrosanti, D., Angelis, M.D. and Basili. M. (2017), "Optimal design and performance evaluation of systems with tuned mass damper inerter (TMDI)", *Earthq. Eng. Struct. Dyn.*, **46**(8), 1367-1388.

Smith, M.C. (2002), "Synthesis of mechanical networks: the inerter", *IEEE Tran. IEEE Trans. Autom. Control.*, **47** 1648-1662.

Sun, C., Eason, R.P., Nagarajaiah, S. and Dick, A.J. (2013), "Hardening Duffing oscillator attenuation using a nonlinear TMD, a semi-active TMD and multiple TMD", *J. Sound Vib.*, **332**(4), 674-686.

Wang, F., Hong, M. and Lin, T. (2010), "Designing and testing a hydraulic inerter", *Proc. Inst. Mech. Eng. Part C: J. Mech. Eng. Sci.*, **225**(1), 66-72.

Xu, K. and Igusa, T. (1992), "Dynamic characteristics of multiple substructures with closely spaced frequencies", *Earthq. Eng. Struct. Dyn.* **21**(12), 1059-1070.

AT

Nomenclature

a_s	Absolute acceleration of the structure
$A_s(s)$	Laplace transform of a_s
a_T	Absolute acceleration of the ATMDI
$A_T(s)$	Laplace transform of a_T
ACF-TF	Active control force transfer function
ATF	Acceleration transfer function
ATMD	Active tuned mass damper
ATMDI	Active tuned mass damper inerter
b	Inertance coefficient
c_s	Viscous damping coefficient of the structure
c_T	Viscous damping coefficient of the ATMDI
$\bar{c}_T$	Feedback gain of velocity of the ATMDI
DMF	Dynamic magnification factors
DMF_{A_s}	DMF of acceleration of the structure
DMF_{F_I}	DMF of inerter element force of the ATMDI
DMF_{U_T}	DMF of active control force of the ATMDI
DMF_{Y_s}	DMF of displacement of the structure
DMF_{Y_T}	DMF of displacement of the mass block of the ATMDI
DTF	Displacement transfer function
FF	Far-field
$f_I(t)$	Inerter element force
$F_I(s)$	Laplace transform of $f_I(t)$
f_T	Tuning frequency ratio of the ATMDI
f_{Topt}	Optimum tuning frequency ratio of the ATMDI
IEF-TF	Inerter element force transfer function
k_s	Stiffness coefficient of the structure
k_T	Stiffness coefficient of the ATMDI
$\bar{k}_T$	Feedback gain of displacement of the ATMDI
max.DMF_{A_s}	Maximum value of acceleration DMF of the structure with the ATMDI taking its respective optimum parameters
max.DMF_{F_I}	Maximum value of inerter element force DMF of the ATMDI taking its respective optimum parameters
max.DMF_{U_T}	Maximum value of active control force DMF of the ATMDI taking its respective optimum parameters
max.DMF_{Y_T}	Maximum value of displacement DMF of the mass block of the ATMDI taking its respective optimum parameters
$MDOF$	Multi-degrees-of-freedom
m_s	Mass of the structure
m_T	Mass of the ATMDI
$\bar{m}_T$	Feedback gain of acceleration of the structure
MTMD	Multiple tuned mass damper
NAFGF	Acceleration feedback gain factors
NF	Near-field
NFE	Nondimensional frequency of excitation
NTMD	Nonlinear tuned mass damper
PSO	Particle swarm optimization
R	Minimization of the maximum values of the DMF of the structure with the ATMDI
SDOF	Single degree-of-freedom
TMD	Tuned mass damper
TMDI	Tuned mass damper inerter
$u_T(t)$	Active control force
$U_T(s)$	Laplace transform of $u_T(t)$
$\ddot{x}_g(t)$	Ground acceleration
$\ddot{X}_g(s)$	Laplace transform of $\ddot{x}_g(t)$
y_s	Relative displacement of the structure with reference to the ground
$Y_s(s)$	Laplace transform of y_s
y_T	Relative displacement of the ATMDI with reference to the structure
$Y_T(s)$	Laplace transform of y_T
α_T	Normalized acceleration feedback gain factors
λ	Nondimensional frequency of excitation
ξ_s	Damping ratio of the structure

ξ_T	Damping ratio of the ATMDI
ξ_{Topt}	Optimum damping ratio of the ATMDI
ξ_{TMDI}	Damping ratio of the TMDI
μ_I	Inerter mass ratio
μ_T	Mass ratio
ω	External excitation frequency
ω_s	Structural natural frequency corresponding to the vibration mode being controlled
ω_T	Natural frequency of the ATMDI
ω_{TMDI}	Natural frequency of the TMDI